Journal of Solid State Chemistry 181 (2008) 3177–3184

Contents lists available at ScienceDirect

Journal of Solid State Chemistry

journal homepage: www.elsevier.com/locate/jssc

Oxygen nonstoichiometry and defect structure analysis of *B*-site mixed perovskite-type oxide (La, Sr)(Cr, *M*)$O_{3-\delta}$ (*M* = Ti, Mn and Fe)

Masatsugu Oishi [a,*], Keiji Yashiro [a], Kazuhisa Sato [a], Junichiro Mizusaki [a], Tatsuya Kawada [b]

[a] Institute of Multidisciplinary Research for Advanced Materials, Tohoku University, 2-1-1 Katahira, Aoba-ku, Sendai 980-8577, Japan
[b] Graduate School of Environmental Studies, Tohoku University, 6-6-01 Aoba, Aramaki, Aoba-ku, Sendai 980-8579, Japan

ARTICLE INFO

Article history:
Received 23 April 2008
Received in revised form
10 August 2008
Accepted 14 August 2008
Available online 20 August 2008

Keywords:
Defect structure
Oxygen nonstoichiometry
Perovskite-type oxides
$LaCrO_3$
B-site mixing
SOFC

ABSTRACT

The defect chemical relationships in various *B*-site mixed $LaCrO_3$-based ceramics were investigated by means of high-temperature gravimetry. The nonstoichiometric deviation, δ, in $(La_{0.7}Sr_{0.3})(Cr_{1-y}Ti_y)O_{3-\delta}$ ($y = 0.1$, 0.2 and 0.3) (LSCT), $(La_{0.75}Sr_{0.25})(Cr_{0.5}Mn_{0.5})O_{3-\delta}$ (LSCM) and $(La_{0.75}Sr_{0.25})(Cr_{0.5}Fe_{0.5})O_{3-\delta}$ (LSCF) were measured as a function of oxygen partial pressure, P_{O_2}, at temperatures between 973 and 1373 K.

The effects of partial replacement of the donor on Cr-sites were examined in LSCT. In LSCM and LSCF, effects of the partial substitution of isovalent transition metals on Cr-sites are discussed. Oxygen nonstoichiometries of various *B*-site mixed $LaCrO_3$-based ceramics were compared with those of *A*-site substituted perovskite-type oxides, $(La_{1-x}Sr_x)MO_{3-\delta}$ (where $x = 0$–0.3, M = Cr, Mn and Fe). The partial substitution of the different elements on Cr-sites drastically changed the P_{O_2} and temperature dependence of oxygen vacancy formation in $LaCrO_3$-based ceramics. The defect equilibrium relationships of the localized electron well explained the oxygen vacancy formation in *B*-site mixed $LaCrO_3$-based ceramics. Oxygen vacancy formation in $(La_{0.7}Sr_{0.3})(Cr_{1-y}Ti_y)O_{3-\delta}$ ($y = 0.1$ and 0.2) and $(La_{0.7}Sr_{0.3})(Cr_{0.7}Ti_{0.3})O_{3-\delta}$ was explained by redox reaction of Cr and Ti ions, respectively. The defect equilibrium relationships of LSCM and LSCF were interpreted by redox reaction of Mn ions and Fe ions, respectively. No significant change in valence state of Cr^{3+} ions in LSCM and LSCF was confirmed under the experimental conditions.

1. Introduction

Perovskite-type oxides have the general formula of ABO_3, comprise various compounds and show various properties such as high electronic conductivity, high ionic conductivity, high catalytic activity, superconductivity, ferro-electricity, magnetism, etc. This allows the perovskite-type oxides to be applied in various fields [1–4]. In the perovskite-type structure, *B*-site metals are in the three-dimensional corner sharing array of the BO_6 octahedron and *A*-site metals are located in the body center surrounded by 12 oxygen ions. The coordination number of oxygen for the *A*-site element is 12 and it is 6 for the *B*-site element. Therefore, the strong bonding between *B*-site ions and oxygen ions essentially determines the basic character of perovskite-type oxides [1–3]. Taking advantage of this nature, *B*-site mixed perovskite-type oxide, $A(B_1,B_2)O_3$, is expected to show the desired properties found both in B_1 and B_2 metal oxides.

In fact, various *B*-site mixed perovskite-type oxides have been reported to show superior property compared to the conventional materials for solid oxide fuel cells (SOFC) applications [4–10]. Tao and Irvine [11] reported that $(La_{0.75}Sr_{0.25})(Cr_{0.5}Mn_{0.5})O_3$ shows anode performance comparable to that of Ni-YSZ cermets. $(La_{1-x}Sr_x)(Co_{1-y}Fe_y)O_{3-\delta}$ has been intensively investigated as the cathode materials for SOFC operated at intermediate temperature [12,13]. $(La_{0.75}Sr_{0.25})(Cr_{0.5}Fe_{0.5})O_{3-\delta}$ was examined as the anode material to show good catalyst performance for methane oxidation [14].

However, most of the studies focus only on the properties of the *B*-sites perovskite-type oxides that the changes of defect structures, phase stability and thermodynamic quantities have rather been neglected. By mixing different elements in the *B*-site, the strong connection of BO_6 may be broken and this leads to the changes in the main framework of perovskite-type oxides. This may cause instability of structures to express negative property changes. Moreover, the defect structure may be really complex compared to that of *A*-site doped perovskite-type oxides.

The defect structure of *B*-site mixed $LaCrO_3$ was investigated by measuring oxygen nonstoichiometry, δ, in $LaCr_{0.9}M_{0.1}O_{3-\delta}$ (M = Ni, Co and Fe) by means of high-temperature gravimetry [15]. They showed that oxygen nonstoichiometry behavior of *B*-site mixed $LaCrO_3$ was different by the different *B*-site species, and it was also different from those of *A*-site doped $LaCrO_3$ [16]. Oxygen vacancy concentration increased in *B*-site mixed $LaCrO_3$ compared to that of *A*-site doped $LaCrO_3$. It was shown that partial replacement of different elements on Cr-sites strongly affects the redox properties of Cr ions and the stability of oxygen vacancy.

* Corresponding author. Fax: +81 22 217 5343.
E-mail address: oishi@mail.tagen.tohoku.ac.jp (M. Oishi).

0022-4596/$ - see front matter © 2008 Elsevier Inc. All rights reserved.
doi:10.1016/j.jssc.2008.08.015

In this work, nonstoichiometric variation of oxygen content in $(La_{0.7}Sr_{0.3})(Cr_{1-y}Ti_y)O_{3-\delta}$ ($y = 0.1$, 0.2 and 0.3) (LSCT), $(La_{0.75}Sr_{0.25})(Cr_{0.5}Mn_{0.5})O_{3-\delta}$ (LSCM) and $(La_{0.75}Sr_{0.25})(Cr_{0.5}Fe_{0.5})O_{3-\delta}$ (LSCF) was measured as a function of oxygen partial pressure, P_{O_2}, at 973–1373 K. The effect of partial replacement of different elements is investigated by comparing oxygen nonstoichiometries of *B*-site mixed and non *B*-site mixed (La,Sr)CrO_3. The defect models are introduced to interpret the results.

2. Experimental

2.1. Sample preparation

Powders of LSCT, LSCM and LSCF were prepared by a solid-state reaction method. La_2O_3 (RARE METALLIC 99.99%), $SrCO_3$ (RARE METALLIC 99.99%), Cr_2O_3 (HIGH PURITY CHEMICALS 99.98%), TiO_2 (HIGH PURITY CHEMICALS 99.99%), Mn_2O_3 (HIGH PURITY CHEMICALS 99.9%) and Fe_2O_3 (HIGH PURITY CHEMICALS 99.9%) were used as starting materials. La_2O_3 powders were annealed in air at 1473 K for 10 h to dry and also reduce the surface area to avoid dehydration during cooling and weighing. The sample was kept in vacuum desiccators during cooling.

The starting powders of each composition were carefully weighed in the appropriate ratio and mixed together using a ball mill. The mixed powders were calcined at 1573 K for 5 h in air. The powder was pulverized and submitted for X-ray diffraction (XRD) analysis. Calcination was repeated until the powder showed only a set of perovskite-type phases.

For high-temperature gravimetry, about 1 g of the pre-calcined powder was pressed into a cylindrical shape under 300 MPa hydrostatic pressure and sintered in air at 1673 K for 3 h. Density of sintered pellets was between 55% and 70%.

2.2. High-temperature gravimetry

Oxygen nonstoichiometry was measured by high-temperature gravimetry using microbalance (Sartorius M25DP). Details of the setup are essentially the same as those given before in [15]. Oxygen partial pressure was controlled by the gas-mixing system for O_2–Ar, CO–CO_2 and H_2–H_2O–Ar. Values of P_{O_2} and temperature were monitored by the oxygen sensor and thermocouple located just below the sample. During measurements, weight change of the sample was continuously monitored as a function of time under the fixed P_{O_2} and temperature. When the weight change reached the stationary value, the equilibrium between the sample and the gas phase was considered to be confirmed.

Oxygen nonstoichiometry, δ, is calculated using the equation

$$\Delta\delta = \frac{M_{\text{sample}}}{M_O w_{\text{sample}}}\Delta w, \tag{1}$$

where Δw is the weight change from the stoichiometric oxygen compositions at the equilibrium with P_{O_2} and temperature. M_O and w_{sample} are molar weight of oxygen atoms and weight of sample, respectively. M_{sample} is the molar weight of the sample at the stoichiometric oxygen composition.

3. Results and discussion

3.1. Oxygen nonstoichiometry of $(La_{0.7}Sr_{0.3})(Cr_{1-y}Ti_y)o_{3-\delta}$ ($y = 0.1$, 0.2 and 0.3)

P_{O_2} dependence of δ in $(La_{0.7}Sr_{0.3})(Cr_{0.9}Ti_{0.1})O_{3-\delta}$ (LSCT7391), $(La_{0.7}Sr_{0.3})(Cr_{0.8}Ti_{0.2})O_{3-\delta}$ (LSCT7382) and $(La_{0.7}Sr_{0.3})(Cr_{0.7}Ti_{0.3})O_{3-\delta}$ (LSCT7373) are shown, respectively, in Fig. 1(a)–(c). The stoichiometric composition is usually determined at P_{O_2}, at which $\partial\Delta\delta/\partial \log P_{O_2}$ value takes the minimum value [17]. In LSCT, the sample weight showed plateau in high P_{O_2} region. Hence, this weight was assigned as the stoichiometric composition ($\delta = 0$) at respective temperatures.

The measured δ increased with the decrease in P_{O_2} and increase in temperature. This behavior is similar to the relationship between oxygen content and P_{O_2} of various Sr acceptor doped $LaCrO_3$ [18]. That is, the loss of the positive charge by partial substitution of the acceptor Sr^{2+} on La^{3+}-sites is compensated by the formation of Cr^{4+} under oxidizing atmospheres. Oxygen vacancy is formed under reducing atmospheres accompanied by the reduction of Cr^{4+} to Cr^{3+} ions [18].

In LSCT, Sr^{2+} ions on La^{3+}-sites work as the acceptor. On the other hand, Ti^{4+} ions on Cr^{3+}-sites work as the donor. For example, in LSCT7382, with 30 mol% of Sr^{2+} as the acceptor and 20 mol% of Ti^{4+} as the donor, the total amount of acceptor content is 10 mol%. Total acceptor contents are the same with $(La_{0.9}Sr_{0.1})CrO_{3-\delta}$. As concentration of oxygen vacancy is determined by electrical neutrality conditions, it is expected that δ values are same in LSCT7382 and $(La_{0.9}Sr_{0.1})CrO_{3-\delta}$. Comparison of oxygen vacancy in LSCT7382 and $(La_{0.9}Sr_{0.1})CrO_{3-\delta}$ [18] is shown in Fig. 2. In Fig. 2, it is shown that the δ values are different in LSCT7382 and $(La_{0.9}Sr_{0.1})CrO_{3-\delta}$ although the total acceptor content is the same. The δ values in LSCT7382 are larger than those in $(La_{0.9}Sr_{0.1})CrO_{3-\delta}$ at respective temperatures. Moreover, δ values in LSCT7391 and $(La_{0.8}Sr_{0.2})CrO_{3-\delta}$, in which both have 20 mol% of total acceptor contents, were also different. The δ values in LSCT7391 were larger compared to those in $(La_{0.8}Sr_{0.2})CrO_{3-\delta}$.

In LSCT7373, amounts of the acceptor and the donor are the same. Therefore, no change from stoichiometric composition was expected, just like the deviation from the stoichiometric composition in pure $LaCrO_3$ is negligibly small. However, as shown in Fig. 1(c), composition of LSCT7373 deviated from the stoichiometric composition and changed as a function of P_{O_2} and temperature.

Weight increase was observed above the stoichiometric composition of LSCT in high P_{O_2} region. Relaxation time of weight changes in high P_{O_2} region was much longer than that in low-P_{O_2} regions where oxygen vacancy is formed. The obtained data above the stoichiometric composition are plotted with the open symbols in Fig. 1. The slow kinetics is regarded to be controlled by the diffusion rate of cations. First, we considered the formation of the second phase, $SrCrO_4$, which is the compound of Cr^{6+} ions. Miyoshi et al. [19] reported that two kinds of the second phase, $SrCrO_4$ and unknown phase were observed in $La_{1-x}Sr_xCrO_3$ ($x = 0$–0.3) (LSC) depending on conditions. The second phases tend to form at low temperature in high P_{O_2} regions and with large Sr contents. As P_{O_2} and temperature conditions at which the slow kinetic was observed in LSCT corresponded to the conditions of the second phase formation in LSC, we considered that second phases are also formed in LSCT.

The LSCT7391, LSCT7382 and LSCT7373 powders were equilibrated at $P_{O_2} = 1$ bar at 973 K at which the weight increase was observed by the high-temperature gravimetry. Powders were kept programmed for 160 h, and subsequently cooled to room temperature within less than 15 min. The obtained samples were evaluated by XRD measurements whether the second phases are formed in LSCT in high P_{O_2} regions. The results prove contrary to our speculations. XRD patterns of all the annealed samples showed only the pattern of the perovskite phase. No second phase was detected in all samples.

Another possibility of the slow cation diffusion is the formation of cation vacancies in *A*- and *B*-sites to show excess oxygen nonstoichiometry. Generally, oxygen excess nonstoichiometry is rarely observed in perovskite-type oxides due to the closely

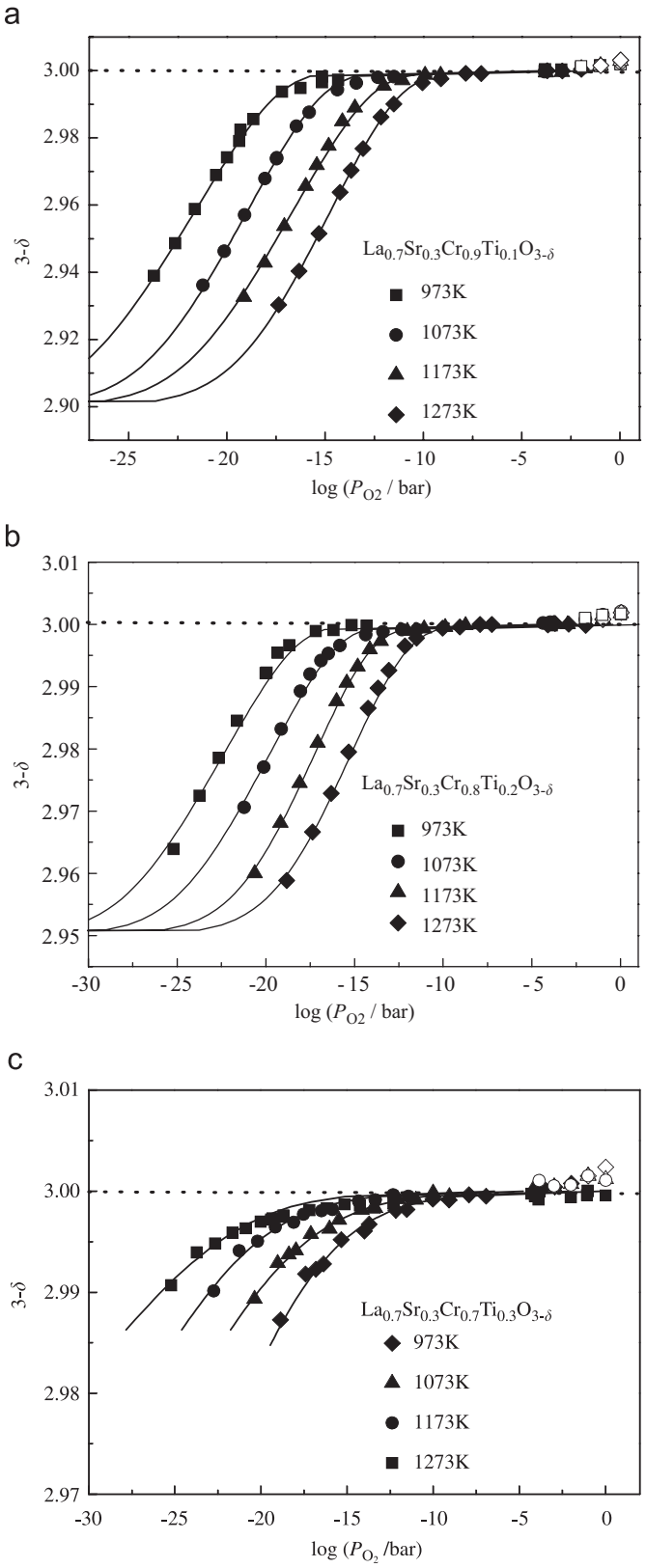

Fig. 1. Oxygen nonstoichiometry of (a) $(La_{0.7}Sr_{0.3})(Cr_{0.9}Ti_{0.1})O_{3-\delta}$, (b) $(La_{0.7}Sr_{0.3})(Cr_{0.8}Ti_{0.2})O_{3-\delta}$ and (c) $(La_{0.7}Sr_{0.3})(Cr_{0.7}Ti_{0.3})O_{3-\delta}$. The data above the stoichiometric composition ($\delta = 0$) are denoted by open symbols.

packed structure. One of the particular perovskite-type oxides to show the oxygen excess nonstoichiometry is $LaMnO_3$-based ceramics [20–22]. The cation vacancy in $LaMnO_3$-based

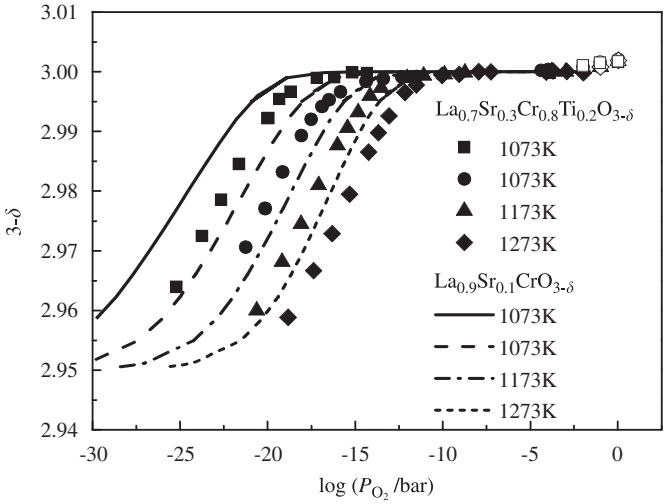

Fig. 2. Oxygen nonstoichiometry of $(La_{0.7}Sr_{0.3})(Cr_{0.8}Ti_{0.2})O_{3-\delta}$ and $(La_{0.9}Sr_{0.1})CrO_{3-\delta}$ [18].

ceramics was experimentally confirmed by the powder neutron diffraction [22].

It is considered that the cation vacancies are likely formed rather than forming Cr^{6+} ions in high P_{O_2} regions in LSCT. This may be explained by the decrease in activity of Cr ions in LSCT by partial substitution of Ti ions on Cr-sites compared to that in LSC where Cr ions are oxidized to form Cr^{6+} ions in high P_{O_2} regions. Further efforts are being made to confirm this behavior. These data points were excluded from the defect structure analysis.

3.2. Oxygen nonstoichiometry of $(La_{0.75}Sr_{0.25})(Cr_{0.5}Mn_{0.5})O_{3-\delta}$ and $(La_{0.75}Sr_{0.25})(Cr_{0.5}Fe_{0.5})O_{3-\delta}$

Fig. 3 shows the P_{O_2} dependence of δ in LSCM and LSCF. The δ values drastically change by the different transition metals substituted on the *B*-site of $LaCrO_3$ and showed larger values compared to those in LSC. Deviation from the stoichiometric composition is larger in LSCF compared to that in LSCM. Thermogravimetric measurement data of LSCF and LSCM showed hysteresis in low-P_{O_2} regions at high temperatures.

In LSCM, sample weight showed plateau in high P_{O_2} region. This weight was assigned as the stoichiometric composition ($\delta = 0$) at respective temperatures, and while in LSCF, no plateau was observed under the measured conditions. Under experimental conditions, LSCF is in the oxygen-deficient state. In order to determine the stoichiometric composition of LSCF, sample weights were measured at temperatures below the experimental temperature [23]. It was found that sample weight measured at $P_{O_2} = 1$ and 10^{-2} bar below 773 K saturated around 473 K. The saturated weights at $P_{O_2} = 1$ and 10^{-2} bar were the same below 473 K. As $\partial\Delta\delta/\partial \log P_{O_2}$ value is considered to be close to zero between $P_{O_2} = 1$ and 10^{-2} bar, the weight under this conditions was determined as the stoichiometric composition of $\delta = 0$. The difference in buoyancy among the different gas and temperature was corrected by measuring the weight change of a dense alumina disk. After the compensation, accuracy of weight change was $\pm 30\,\mu g$, which is $\delta = \pm 0.0007$. The errors of δ values in LSCF were within the size of the symbols in Fig. 3.

The P_{O_2} dependence of δ in LSCM at 1173 K is shown along with the oxygen nonstoichiometry of $(La_{0.75}Sr_{0.25})CrO_{3-\delta}$ (LSC25) [18] and $(La_{0.75}Sr_{0.25})MnO_{3-\delta}$ (LSM25) [21] in Fig. 4(a). Relationships between δ and P_{O_2} in LSCM are similar to those in LSM25. Oxygen nonstoichiometry behavior of LSCM deviated from that of LSM25 in low-P_{O_2} regions.

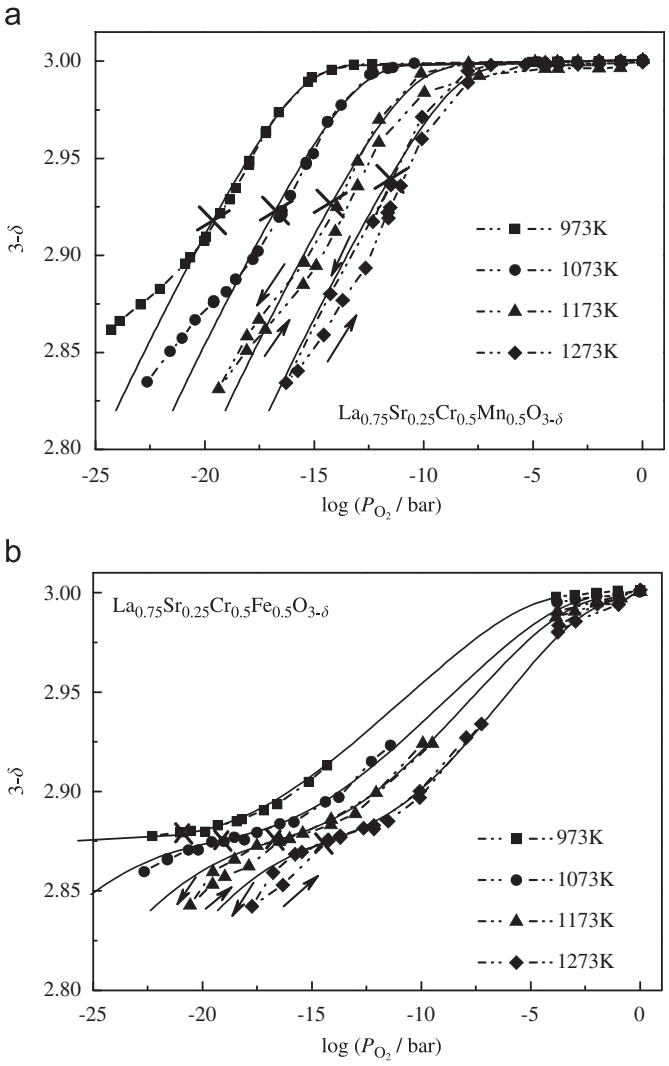

Fig. 3. Oxygen nonstoichiometry of (a) $(La_{0.75}Sr_{0.25})(Cr_{0.5}Mn_{0.5})O_{3-\delta}$ and (b) $(La_{0.75}Sr_{0.25})(Cr_{0.5}Fe_{0.5})O_{3-\delta}$. The decomposition P_{O_2} of $La_{0.7}Sr_{0.3}MnO_{3-\delta}$ [21] and FeO are indicated with the cross symbols in (a) and (b) respectively.

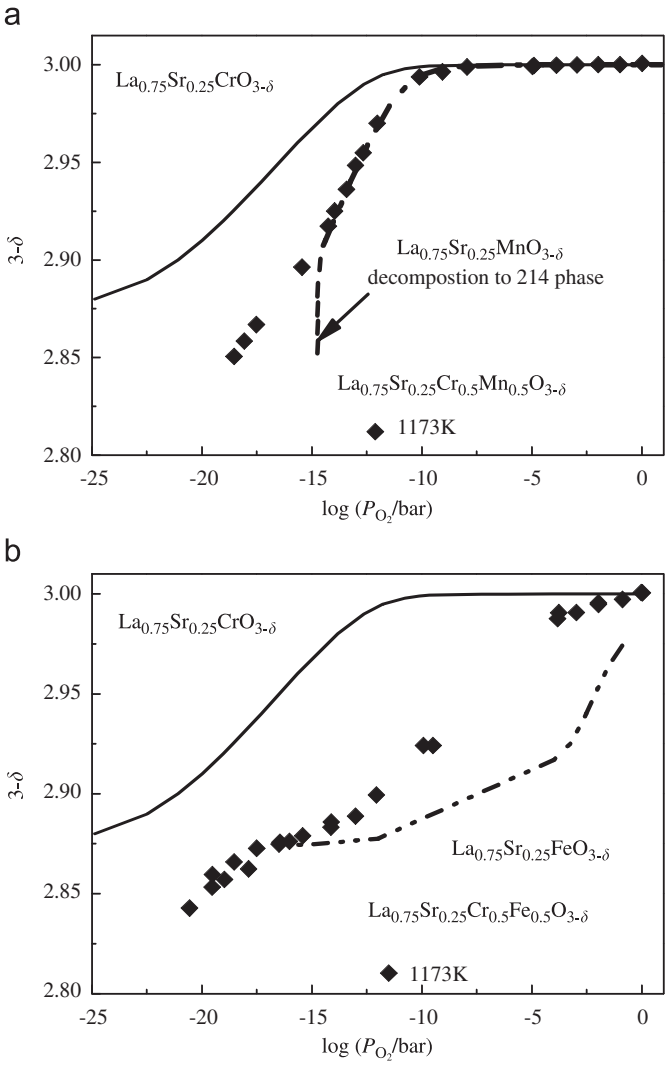

Fig. 4. Comparison of the oxygen nonstoichiometry between (a) $(La_{0.75}Sr_{0.25})(Cr_{0.5}Mn_{0.5})O_{3-\delta}$, $(La_{0.75}Sr_{0.25})CrO_{3-\delta}$ [18] and $(La_{0.75}Sr_{0.25})MnO_{3-\delta}$ [21], and (b) $(La_{0.75}Sr_{0.25})(Cr_{0.5}Fe_{0.5})O_{3-\delta}$, $(La_{0.75}Sr_{0.25})CrO_{3-\delta}$ [18] and $(La_{0.75}Sr_{0.25})FeO_{3-\delta}$ [23] at 1173 K.

In Fig. 4(b) shows the P_{O_2} dependence of δ in LSCF at 1173 K compared with that of LSC25 and $(La_{0.75}Sr_{0.25})FeO_{3-\delta}$ (LSF25) [23]. The nonstoichiometry curve of LSCF is observed between those of LSC25 and LSF25.

Both LSCM and LSCF showed hysteresis in low-P_{O_2} region above 1173 K. Quenched samples of different P_{O_2} at 1173 K were prepared for X-ray analysis. In the XRD pattern of LSCM quenched at $P_{O_2} = 10^{-20}$ bar and 1173 K showed second phases of $(La,Sr)_2MnO_4$ and MnO (Fig. 5(a)). It has been reported by Mizusaki et al. [21] that $La_{1-x}Sr_xMnO_{3-\delta}$ (LSM) decompose under reducing atmospheres. Decomposition P_{O_2} of LSM is indicated with cross symbols on the thermogravimetric data of LSCM in Fig. 3(a). Under the reducing atmosphere below decomposition P_{O_2}, LSCM is considered to be in the quasi-stable conditions of LSCM phase and the second phases. The hysteresis is considered to be due to the slow equilibriums of the decomposition reaction.

In the XRD pattern of LSCF quenched at $P_{O_2} = 10^{-20}$ bar and 1173 K, the second phase of $(La,Sr)_2FeO_4$ is also recognized (Fig. 5(b)). The equilibrium P_{O_2} of $2FeO = 2Fe+O_2$ are indicated in Fig. 3(b) with cross symbols on the thermogravimetric data of LSCF at respective temperatures. The P_{O_2} regions at which the hysteresis is recognized are below the equilibrium P_{O_2} of the reaction between FeO and Fe. Therefore, the hysteresis is considered to be due to phase separation due to reduction of Fe ions under the reducing atmosphere.

To further understand the stability of LSCT, LSCM and LSCF, investigation of XRD as the functions of composition, P_{O_2} and temperature would provide valuable information. This is the forthcoming subject of this study.

3.3. Defect structure analysis

3.3.1. Defect chemical equilibrium in $(La_{0.7}Sr_{0.3})(Cr_{1-y}Ti_y)O_{3-\delta}$ ($y = 0.1$, 0.2 and 0.3)

Vashook et al. [24,25] investigated the electrical conductivities of a series of perovskite-type compounds $La_{1-x}Ca_xCr_{1-y}Ti_yO_{3-\delta}$ with $x = 0$–1 and $y = 0$–1 taking them as the functions of composition, temperature and P_{O_2}. They reported that the compounds of $x > y$ were p-type and of $x \leqslant y$ were n-type semiconductors. The p-type conduction of the compounds of $x > y$ was considered to be due to the valence change of Cr ions between Cr^{4+} and Cr^{3+} ions. On the other hand, the n-type conduction of compounds satisfying $x \leqslant y$ was considered to be due to the valence change of Ti ions between Ti^{4+} and Ti^{3+} ions. Here, the defect chemical equilibriums in $La_{1-x}Sr_xCr_{1-y}Ti_yO_{3-\delta}$ with $x = 0.3$ and $y = 0$–0.3

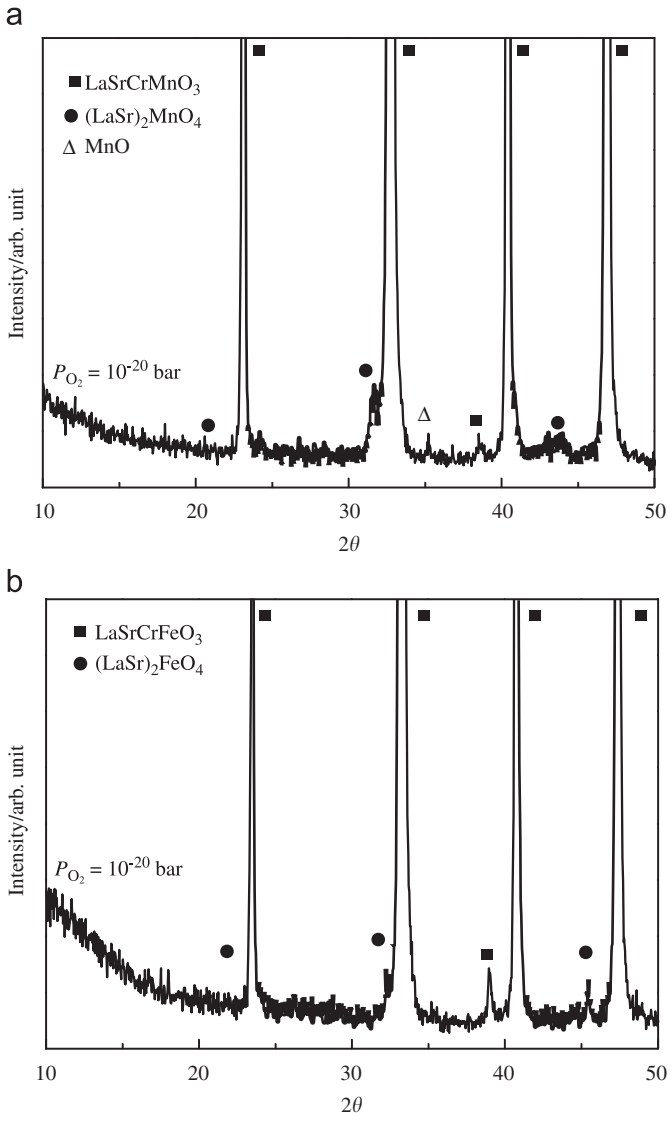

Fig. 5. The XRD pattern of quenched sample at $P(O_2) = 10^{-20}$ bar and 1173 K of (a) $(La_{0.75}Sr_{0.25})(Cr_{0.5}Mn_{0.5})O_{3-\delta}$ and (b) $(La_{0.75}Sr_{0.25})(Cr_{0.5}Fe_{0.5})O_{3-\delta}$.

are discussed to explain the results of the thermogravimetric measurements and thermodynamic parameters are calculated.

(i) $x>y$: LSCT7391 and LSCT7382

The defect chemical equilibriums for LSCT7391 and LSCT7382 are considered among Sr'_{La}, $V_O^{\bullet\bullet}$, $Cr_{Cr}^{\times}$, $Cr_{Cr}^{\bullet}$, $O_O^{\times}$ and $Ti_{Cr}^{\bullet}$, where Sr'_{La} indicates the Sr^{2+} ion in La^{3+}-sites, $V_O^{\bullet\bullet}$ indicates the introduced oxygen vacancy, $Cr_{Cr}^{\times}$ indicates Cr^{3+} ions in Cr^{3+}-sites, $Cr_{Cr}^{\bullet}$ indicates Cr^{4+} ions in Cr^{3+}-sites, $O_O^{\times}$ indicates an oxygen ion in oxygen sites, and $Ti_{Cr}^{\bullet}$ indicates Ti^{4+} ions in Cr^{3+}-sites. The Kröger–Vink-type notation is used in this paper to describe the defect species [26].

The exchange of oxygen between LSCT and a gas phase is described by the quasi-chemical equation

$$2Cr_{Cr}^{\times} + V_O^{\bullet\bullet} + \tfrac{1}{2}O_2(g) = 2Cr_{Cr}^{\bullet} + O_O^{\times}. \tag{2}$$

The equilibrium constant, K_{OX}, for this reaction can be expressed by

$$K_{OX} = \frac{a_{O_O^{\times}} a_{Cr_{Cr}^{\bullet}}^2}{a_{V_O^{\bullet\bullet}} a_{Cr_{Cr}^{\times}}^2} P_{O_2}^{-1/2} = \frac{[O_O^{\times}][Cr_{Cr}^{\bullet}]^2}{[V_O^{\bullet\bullet}][Cr_{Cr}^{\times}]^2} \frac{\gamma_3\gamma_4^2}{\gamma_1\gamma_2^2} P_{O_2}^{-1/2} \tag{3}$$

where $a_{V_O^{\bullet\bullet}}$, $a_{Cr_{Cr}^{\times}}$, $a_{O_O^{\times}}$, $a_{Cr_{Cr}^{\bullet}}$ and γ_1, γ_2, γ_3, γ_4 are activity and activity coefficients of $V_O^{\bullet\bullet}$, $Cr_{Cr}^{\times}$, $O_O^{\times}$, $Cr_{Cr}^{\bullet}$, respectively.

The conditions of charge neutrality is given by

$$[Sr'_{La}] = 2[V_O^{\bullet\bullet}] + [Cr_{Cr}^{\bullet}] + [Ti_{Cr}^{\bullet}] \tag{4}$$

Further, the number of the *B*-site cation ion site is maintained as 1, and therefore

$$[Cr_{Cr}^{\times}] + [Cr_{Cr}^{\bullet}] + [Ti_{Cr}^{\bullet}] = 1. \tag{5}$$

With Eqs. (4) and (5), and the following definitions:

$$[Ti_{Cr}^{\bullet}] = y, \tag{6}$$

$$[Sr'_{La}] = x, \tag{7}$$

$$[V_O^{\bullet\bullet}] = \delta, \tag{8}$$

$$[O_O^{\times}] = 3 - \delta, \tag{9}$$

we obtain

$$[Cr_{Cr}^{\bullet}] = x - y - 2\delta, \tag{10}$$

$$[Cr_{Cr}^{\times}] = 1 - x + 2\delta. \tag{11}$$

From Eqs. (3), (8)–(11), we get

$$\begin{aligned}\Delta G^{\circ} = \Delta H^{\circ} - T\Delta S^{\circ} &= -RT \ln K_{OX} \\ &= -RT \ln\left(\left(\frac{3-\delta}{\delta}\right)\left(\frac{x-y-2\delta}{1-x+2\delta}\right)^2 P_{O_2}^{-1/2}\right) \\ &\quad - RT \ln\left(\frac{\gamma_3\gamma_4^2}{\gamma_1\gamma_2^2}\right)\end{aligned} \tag{12}$$

where ΔG°, ΔH° and ΔS° are, respectively, the standard free energy change, standard enthalpy change and standard entropy change of reaction (2).

The second term in Eq. (12) is defined as the deviation from the standard free energy change of the ideal solution, ΔG_{dev}, and is given as a linear function of oxygen nonstoichiometry

$$\Delta G_{dev} = RT \ln\left(\frac{\gamma_3\gamma_4^2}{\gamma_1\gamma_2^2}\right) = a\delta, \tag{13}$$

where a is a constant representing the interaction among lattice ions and defects [15,16]. From Eqs. (12) and (13), the relation between δ and P_{O_2} is expressed by

$$P_{O_2} = \left(\frac{1}{K_{OX}}\right)^2 \left(\frac{3-\delta}{\delta}\right)^2 \left(\frac{x-y-2\delta}{1-x+2\delta}\right)^4 \left(\exp\left(\frac{a\delta}{RT}\right)\right)^2. \tag{14}$$

Fitting parameters of K_{OX} and a are evaluated using the relationship between δ and P_{O_2} at each temperature by least-squares methods. Theoretical curves calculated by the fitted K_{OX} and a values using Eq. (14) are plotted with solid lines in Fig. 1. Theoretical curves showed good agreement with experimental results of LSCT7391 and LSCT7382. The fitted K_{OX} and the a values are shown in Fig. 6. The error bars of K_{OX} were mostly within the size of the symbols. K_{OX} values of LSCT7391 and LSCT7382 were slightly smaller compared to those of LSC.

(ii) $x = y$: LSCT7373

In LSCT7373, the defect chemical equilibriums are considered among Sr'_{La}, $V_O^{\bullet\bullet}$, $Ti_{Cr}^{\times}$, $Ti_{Cr}^{\bullet}$, $O_O^{\times}$ and $Cr_{Cr}^{\times}$, where $Ti_{Cr}^{\times}$ indicates Ti^{3+} ions in Cr^{3+}-sites. The exchange of oxygen between LSCT7373 and a gas phase is described by the following quasi-chemical equation:

$$2Ti_{Cr}^{\times} + V_O^{\bullet\bullet} + \tfrac{1}{2}O_2(g) = 2Ti_{Cr}^{\bullet} + O_O^{\times}. \tag{15}$$

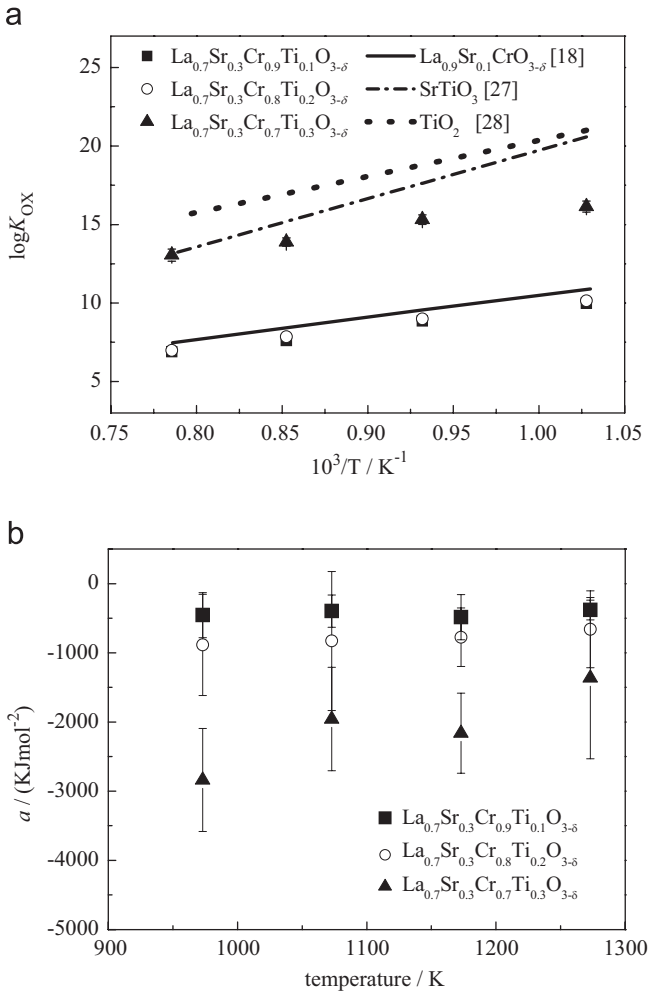

Fig. 6. The equilibrium constants, K_{OX}, and a of $(La_{0.7}Sr_{0.3})(Cr_{0.9}Ti_{0.1})O_{3-\delta}$, $(La_{0.75}Sr_{0.25})(Cr_{0.8}Ti_{0.2})O_{3-\delta}$ and $(La_{0.7}Sr_{0.3})(Cr_{0.7}Ti_{0.3})O_{3-\delta}$. The reported K_{OX} of $La_{0.9}Sr_{0.1}CrO_{3-\delta}$ [18], $SrTiO_3$ [27] and TiO_2 [28] is shown for comparison.

The equilibrium constant, K_{OX}, in Eq. (15) is given by

$$K_{OX} = \frac{a_{O_O^\times} a^2_{Ti_{Cr}^\bullet}}{a_{V_O^{\bullet\bullet}} a^2_{Ti_{Cr}^\times}} P_{O_2}^{-1/2} = \frac{[O_O^\times][Ti_{Cr}^\bullet]^2}{[V_O^{\bullet\bullet}][Ti_{Cr}^\times]^2} \frac{\gamma_3\gamma_6^2}{\gamma_1\gamma_5^2} P_{O_2}^{-1/2} \quad (16)$$

where $a_{Ti_{Cr}^\times}$, $a_{Ti_{Cr}^\bullet}$ and γ_5, γ_6, are activity and activity coefficients of $Ti_{Cr}^\times$ and $Ti_{Cr}^\bullet$, respectively.

The conditions of charge neutrality is given again by

$$[Sr'_{La}] = 2[V_O^{\bullet\bullet}] + [Ti_{Cr}^\bullet]. \quad (17)$$

Further, *B*-site balance is

$$[Cr_{Cr}^\times] + [Ti_{Cr}^\times] + [Ti_{Cr}^\bullet] = 1. \quad (18)$$

We obtain

$$[Ti_{Cr}^\bullet] = x - 2\delta, \quad (19)$$

$$[Ti_{Cr}^\times] = y - x + 2\delta. \quad (20)$$

From Eqs. (7)–(9), (16), (18)–(20), the relationship between δ and P_{O_2} is given by

$$P_{O_2} = \left(\frac{1}{K_{OX}}\right)^2 \left(\frac{3-\delta}{\delta}\right)^2 \left(\frac{x-2\delta}{y-x+2\delta}\right)^4 \left(\exp\left(\frac{a\delta}{RT}\right)\right)^2. \quad (21)$$

Substituting $x = 0.3$ and $y = 0.3$ in Eq. (21), K_{OX} and a values are evaluated using Eq. (21) for LSCT7373 at each temperature by the least-squares method. Theoretical curves calculated using the fitted K_{OX} and a are plotted with the solid lines in Fig. 1(c). The theoretical curves show good agreement with the experimental results under different temperatures. The K_{OX} and a values are shown in Fig. 6.

In LSCT7373, the redox reaction of the Cr ions may also need to be considered other than that of the Ti ions. As is typically seen on the Ellingham diagram, the equilibrium P_{O_2} of Ti^{4+}/Ti^{3+} is much higher than that for Cr^{3+}/Cr metal. Therefore, the Ti^{4+} ions in LSCT7373 are considered to be reduced before the reduction of the Cr^{3+} ions. As the experimental P_{O_2} conditions in this study were above the equilibrium P_{O_2} of Cr^{3+}/Cr metal at respective temperatures, it is unlikely to consider the contribution of Cr^{3+}/Cr^{2+} couple under the experimental conditions. Moreover, so far the authors recognize, high-temperature equilibrium in the chromium related oxides, no report confirmed the Cr^{2+} states. Therefore, it is considered that the valence state of Cr ions is above the trivalent state under the experimental conditions. It is shown Fig. 1(c) that the theoretical curve deviates from the experimental results at the lower temperature near the stoichiometric composition. The contribution of Cr^{4+}/Cr^{3+} couple may need to be considered to fully explain the defect structure of LSCT7373. Further efforts to understand this behavior are being pursued.

The K_{OX} values of LSCT7373 are larger compared to those of LSCT7391 and LSCT7382. This indicates that oxygen vacancy is easily formed in LSCT7391 and LSCT7382 compared to that in LSCT7373. For comparison, K_{OX} values of $SrTiO_3$ [27] and TiO_2 [28] are also plotted in Fig. 6. K_{OX} values of $SrTiO_3$ and TiO_2 are calculated for the defect chemical relationships of

$$\tfrac{1}{2}O_2 + V_O^{\bullet\bullet} + 2e' = O_O^\times. \quad (22)$$

The K_{OX} values of LSCT7373, $SrTiO_3$ and TiO_2 are calculated from the defect chemical equilibriums considering the changes in the valence state of Ti ions. However, the nature of electronic defects is different in these oxides as the electrons are localized on Ti ions in LSCT7373, while electrons are delocalized in $SrTiO_3$ and TiO_2. The K_{OX} values of LSCT7373 showed values comparable to that of $SrTiO_3$ and TiO_2, but gradients of K_{OX} against the reciprocal temperature were different between the localized LSCT7373 and delocalized $SrTiO_3$ and TiO_2. This indicates that the entropy of the oxygen vacancy formation in LSCT7373, $SrTiO_3$ and TiO_2 is almost the same for the localized and delocalized charge carriers, while the enthalpy is different between the localized and delocalized charge carriers.

3.3.2. *Defect chemical equilibrium in $(La_{0.75}Sr_{0.25})(Cr_{0.5}Mn_{0.5})O_{3-\delta}$*

The valence change of the Cr and Mn ions is considerable to interpret the change of δ as the functions of P_{O_2} and temperature in LSCM. X-ray absorption spectroscopy experimental results of LSCM reported by Plint et al. [29] showed that compensation of Sr and oxygen vacancy formation is associated only by Mn ions. The Cr ions stayed as the trivalent states unchanged in different Sr contents. Therefore, in this study, only valence change of Mn ion is considered and valence state of Cr ion is assumed to be stable as the trivalent state. Therefore, the defect chemical equilibriums in LSCM are considered among Sr'_{La}, $V_O^{\bullet\bullet}$, $O_O^\times$, $Mn_{Mn}^\times$, $Mn_{Mn}^\bullet$, Mn'_{Mn} and $Cr_{Cr}^\times$, where $Mn_{Mn}^\times$ indicates Mn^{3+} in Mn^{3+}-sites, $Mn_{Mn}^\bullet$ indicates Mn^{4+} in Mn^{3+}-sites and Mn'_{Mn} indicates Mn^{2+} in Mn^{3+}-sites.

The exchange of oxygen between LSCM and gas phase is expressed by the two defect chemical relationships:

$$\tfrac{1}{2}O_2 + V_O^{\bullet\bullet} + 2Mn_{Mn}^\times = O_O^\times + 2Mn_{Mn}^\bullet, \quad (23)$$

$$\tfrac{1}{2}O_2 + V_O^{\bullet\bullet} + 2Mn'_{Mn} = O_O^\times + 2Mn_{Mn}^\times. \quad (24)$$

From the experimental facts, it is considered that the effective carrier band of e_g level is close between Mn^{2+}, Mn^{3+} and Mn^{4+}.

Therefore, the disproportionation freely occurs between Mn ions. Mizusaki et al. [21] proposed the defect model of LSM considering the electronic configuration term, which is calculated by concentrations of the related defects. From Eqs. (23) and (24), the relation between δ and P_{O_2} is obtained as

$$\frac{1}{2}\log P_{O_2} + \log\left(\frac{\delta}{3-\delta}\right) = -\log K_{OX} + \log(EC), \tag{25}$$

$$\log(EC) = \left(\frac{[Mn^{\bullet}_{Mn}]}{[Mn^{\bullet}_{Mn}] + [Mn'_{Mn}]}\right)\log\left(\frac{[Mn^{\bullet}_{Mn}]^2}{[Mn^{\times}_{Mn}]^2}\right) + \left(\frac{[Mn'_{Mn}]}{[Mn^{\bullet}_{Mn}] + [Mn^{\times}_{Mn}]}\right)\log\left(\frac{[Mn^{\times}_{Mn}]^2}{[Mn'_{Mn}]^2}\right) \tag{26}$$

where log(EC) denotes the configuration energy of the electronic defects. Considering the site restriction of the Mn ions in the *B*-sites, we have

$$[Mn^{\times}_{Mn}] + [Mn'_{Mn}] + [Mn^{\bullet}_{Mn}] = 0.5. \tag{27}$$

The defect distribution calculation procedure discussed in Ref. [21] leads the concentrations of Mn ions of different valence state as follows:

$$[Mn'_{Mn}] = \frac{6 - 18x + 36\delta}{2(17 - x + 2\delta)}, \tag{28}$$

$$[Mn^{\bullet}_{Mn}] = \frac{-(x+2\delta)^2 - x + 2\delta + 6}{2(17 - x + 2\delta)}, \tag{29}$$

$$[Mn^{\times}_{Mn}] = \frac{(x+2\delta)^2 + 18(x - 2\delta) + 5}{2(17 - x + 2\delta)}, \tag{30}$$

Using Eqs. (7)–(9), (26), (28)–(30), the theoretical relationship between δ and P_{O_2} was obtained from Eq. (25). The deviation from the ideal solution is implemented in the fitting parameter K_{OX} as a linear function of δ with parameter *a*. The fit results are shown by the solid lines in Fig. 3(a). The fitted curves showed good agreement with the experimental results of LSCM between high P_{O_2} and intermediate P_{O_2} ranges. Calculated K_{OX} and *a* values are shown in Fig. 7. The theoretical curves deviate from experimental results in the low P_{O_2} regions as the thermogravimetric measurement data in low P_{O_2} regions reflect not only the composition changes of LSCM but also formation of the second phases.

In LSCM, we have also examined the defect chemical equilibriums of the redox couple of Cr^{4+}/Cr^{3+}. However, the oxygen nonstoichiometry behavior could not be explained by considering defect models of localized electron among Cr^{4+} and Cr^{3+} ions. When considering the electronic structure of Cr^{3+} and Mn^{4+} ions, the Mn e_g-levels are partially filled as opposed to a filled Cr t_{2g}-level. It is considered that the small polaron hopping takes place primarily on the partially filled Mn e_g-levels. Therefore, Mn ions disproportionate among Mn^{3+}, Mn^{4+} and Mn^{2+}, while Cr ions stay as Cr^{3+} states.

3.3.3. *Defect chemical equilibrium in* $(La_{0.75}Sr_{0.25})(Cr_{0.5}Fe_{0.5})O_{3-\delta}$

In LSCF, the defect chemical equilibriums were considered among Sr'_{La}, $V^{\bullet\bullet}_O$, $O^{\times}_O$, $Fe^{\times}_{Fe}$, $Fe^{\bullet}_{Fe}$, Fe'_{Fe} and $Cr^{\times}_{Cr}$, where $Fe^{\times}_{Fe}$ indicates Fe^{3+} in Fe^{3+}-sites, $Fe^{\bullet}_{Fe}$ indicates Fe^{4+} ions in Fe^{3+}-sites and Fe'_{Fe} indicates Fe^{2+} ion in Fe^{3+}-sites. The valence state of the Cr ion is considered to be stable as the trivalent state.

The reaction between oxygen gas and defects in LSCF can be expressed through

$$\tfrac{1}{2}O_2 + V^{\bullet\bullet}_O + 2Fe^{\times}_{Fe} = O^{\times}_O + 2Fe^{\bullet}_{Fe}, \tag{31}$$

$$K_{OX} = \frac{[O^X_O][Fe^{\bullet}_{Fe}]^2}{P^{1/2}_{O_2}[V^{\bullet\bullet}_O][Fe^{\times}_{Fe}]^2} \tag{32}$$

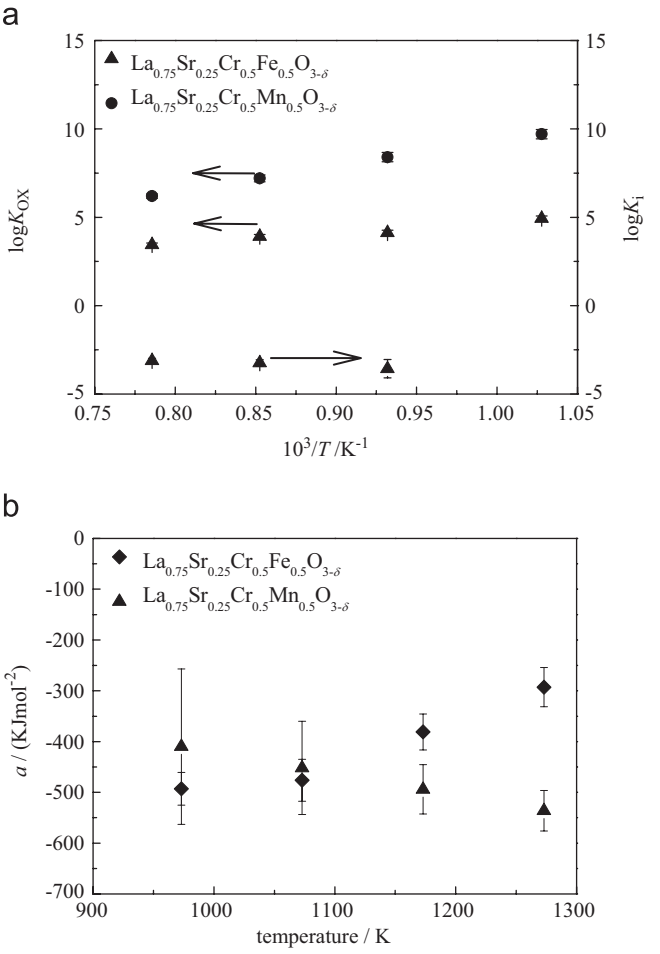

Fig. 7. Equilibrium constants, K_{OX}, and *a* of $(La_{0.75}Sr_{0.25})(Cr_{0.5}Mn_{0.5})O_{3-\delta}$ and $(La_{0.75}Sr_{0.25})(Cr_{0.5}Fe_{0.5})O_{3-\delta}$.

where K_{OX} is the equilibrium constant of Eq. (31). The disproportionation of $Fe^{\times}_{Fe}$ is given by

$$2Fe^{\times}_{Fe} = Fe'_{Fe} + Fe^{\bullet}_{Fe}, \tag{33}$$

$$K_i = \frac{[Fe^{\bullet}_{Fe}][Fe'_{Fe}]}{[Fe^{\times}_{Fe}]^2} \tag{34}$$

where K_i is the equilibrium constant of Eq. (33). The condition of charge neutrality is given by the relation

$$[Sr'_{La}] + [Fe'_{Fe}] = 2[V^{\bullet\bullet}_O] + [Fe^{\bullet}_{Fe}]. \tag{35}$$

The site restriction in LSCF is determined by the given *B*-site composition as follows:

$$[Fe^{\times}_{Fe}] + [Fe'_{Fe}] + [Fe^{\bullet}_{Fe}] = 0.5, \tag{36}$$

$$[Cr^{\times}_{Cr}] = 0.5. \tag{37}$$

From Eqs. (7)–(9), (32), (34)–(37), relationship between δ and P_{O_2} for a general formula of $(La_{1-x}Sr_x)(Cr_{1-y}Fe_y)O_{3-\delta}$ is given by

$$\frac{(2\delta - x + 0.5)\delta^{1/2}}{(2\delta - x)(3-\delta)^{1/2}}P^{1/4}_{O_2} = \frac{K_i}{K_{OX}}\frac{(3-\delta)^{1/2}(x + 0.5 - 2\delta)}{(2\delta - x)\delta^{1/2}P^{1/4}_{O_2}} - K^{-1/2}_{OX} \tag{38}$$

The interaction among the lattice ion and defects is included in K_{OX} as a linear function of δ of parameter *a*. The theoretical curves calculated for LSCF ($x = 0.5$, $y = 0.5$) by the fitted K_{OX}, K_i and *a* values using Eq. (38) are plotted with solid lines in Fig. 3(b). The theoretical curves showed good agreement with the experimental

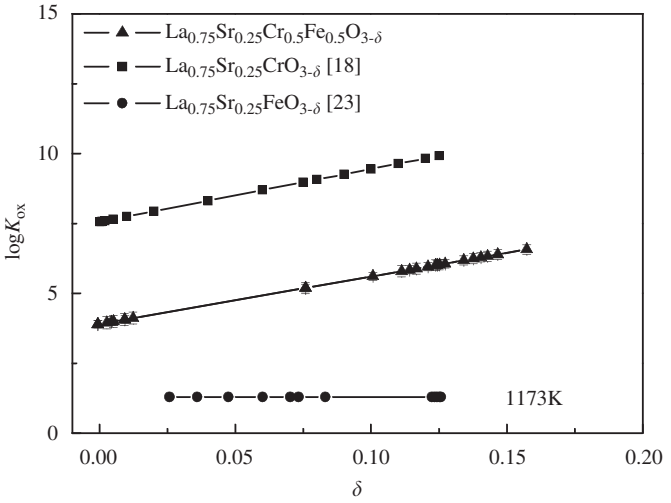

Fig. 8. Equilibrium constants, K_{OX}, as a function of ≅ of $(La_{0.75}Sr_{0.25})(Cr_{0.5}Fe_{0.5})O_{3-\cong}$, $(La_{0.75}Sr_{0.25})CrO_{3-\delta}$ [18], and $(La_{0.75}Sr_{0.25})FeO_{3-\delta}$ [23] at 1173 K.

results of LSCF. The fitted K_{OX}, K_i and a are shown in Fig. 7. The theoretical curves deviated from the experimental results in low-P_{O_2} regions. This is interpreted by decomposition of LSCF into $(La,Sr)_2FeO_4$ and iron oxides already expressed in Section 3.2.

The same defect model of the localized electron is applied in LSCF, LSC and LSF. The equilibrium constants of oxygen vacancy formation in LSCF, LSC and LSF are given as a function of δ in Fig. 8. The best fitted K_{OX} of LSCF is between that of LSC25 and LSF25, which is consistent with oxygen nonstoichiometry results. Slope of K_{OX} against δ indicates the interaction among lattice ions and defects. Similar values are observed for LSCF and LSC25.

4. Conclusions

The oxygen vacancy formation in various *B*-site mixed $LaCrO_3$-based ceramics of different compositions was investigated as a function of P_{O_2} at different temperatures by means of high-temperature gravimetry methods. The oxygen nonstoichiometry of *B*-site mixed $(La,Sr)CrO_3$ strongly depended on the nature of *B*-site dopants.

The defect models which describe the oxygen vacancy formation in various *B*-site mixed $LaCrO_3$-based ceramics were developed and the thermodynamic quantities were compared with various perovskite-type oxides. The charge compensation of the acceptor and donor in LSCT was explained by redox reaction between Cr^{4+} and Cr^{3+} in LSCT7391 and LSCT7382, and between Ti^{4+} and Ti^{3+} in LSCT7373. In LSCF and LSCM, the valence state of Cr^{3+} does not change significantly under experimental P_{O_2} and temperature ranges. In contrast to this, valence state of Mn and Fe ions changed to disproportionate into 4+, 3+ and 2+ oxidation states to compensate for the loss of positive charge of Sr^{2+} in La^{3+}-sites in LSCM and LSCF, respectively.

In LSCT, the weight gradually increased in high P_{O_2} region. This is considered to be due to the formation of the cation vacancy. On the other hands, in LSCM and LSCF, the weight gradually decreased under the reducing atmosphere at high temperatures. This was interpreted by formation of second phases.

Acknowledgment

This work was supported by the Grant-in-aid for Scientific Research on Priority Area, "Nanoionics (439)" by the Ministry of Education, Culture, Sports, Science, and Technology of Japan.

References

[1] W.D. Kingery, H.K. Bowen, D.R. Uhlmann, Introduction to Ceramics, 2nd ed, Wiley, New York, 1976.
[2] Perovskite-Related Compounds: Storehouse of Functions, Nihon kagaku kai, 1997.
[3] P. Kofstad, Nonstoichiometry, Diffusion, and Electrical Conductivity in Binary Metal Oxides, Wiley, New York, 1972.
[4] M.H.R. Lankhorst, J.E. ten Elshof, J. Solid State Chem. 130 (1997) 302.
[5] I. Yasuda, T. Oigawara, H. Yakabe, In: Electrochemical Society Proceedings of the Seventh International Symposium on SOFC, Tsukuba, Japan, 2001, 783pp.
[6] J. Sfeir, P.A. Buffat, P. Mockli, N. Xanthopoulos, R. Vasquez, H.J. Mathieu, J. Van herle, K. Ravindranathan Thampi, J. Catal. 202 (2001) 229.
[7] R. Raffaelle, H.U. Anderson, D.M. Sparlin, P.E. Parris, Phys. Rev. B 43 (1991) 7991.
[8] W.J. Weber, C.W. Griffin, J.L. Bates, J. Am. Ceram. Soc. 70 (1987) 265.
[9] R. Koc, H.U. Anderson, J. Mater. Sci. Soc. 27 (1992) 5477.
[10] R. Koc, H.U. Anderson, J. Eur. Ceram. Soc. 15 (1995) 867.
[11] S. Tao, J.T.S. Irvine, Nat. Mater. 2 (2003) 320.
[12] L.W. Tai, M.M. Nasrallah, H.U. Anderson, D.M. Sparlin, Solid State Ionics 76 (1995) 273.
[13] B.C.H. Steele, J.M. Bae, Solid State Ionics 106 (1998) 255.
[14] S. Tao, J.T.S. Irvine, Chem. Mater. 16 (2004) 4116.
[15] M. Oishi, K. Yashiro, J. Hong, Y. Nigara, T. Kawada, J. Mizusaki, Solid State Ionics 178 (2007) 307.
[16] S. Onuma, K. Yashiro, S. Miyoshi, A. Kaimai, H. Matsumoto, Y. Nigara, T. Kawada, J. Mizusaki, K. Kawamura, N. Sakai, H. Yokokawa, Solid State Ionics 174 (2004) 287.
[17] C. Wagner, Prog. Solid State Chem. 6 (1971) 1.
[18] J. Mizusaki, S. Yamauchi, K. Fueki, A. Ishikawa, Solid State Ionics 12 (1984) 119.
[19] S. Miyoshi, S. Onuma, A. Kaimai, H. Matsumoto, K. Yashiro, T. Kawada, J. Mizusaki, H. Yokokawa, J. Solid State Chem. 177 (2004) 4112.
[20] J.H. Kuo, H.U. Anderson, D.M. Sparling, J. Solid State Chem. 83 (1989) 52.
[21] J. Mizusaki, N. Mori, H. Takai, Y. Yonemura, H. Minamiue, H. Tagawa, M. Dokiya, H. Inaba, K. Naraya, T. Sasamoto, T. Hashimoto, Solid State Ionics 129 (2000) 163.
[22] B.C. Tofield, W.R. Scott, J. Solid State Chem. 10 (1974) 183.
[23] J. Mizusaki, M. Yoshihiro, S. Yamauchi, K. Fueki, J. Solid State Chem. 58 (1985) 257.
[24] V. Vashook, L. Vasylechko, J. Zosel, W. Gruner, H. Ullmann, U. Guth, J. Solid State Chem. 177 (2004) 3784.
[25] V. Vashook, L. Vasylechko, J. Zosel, W. Gruner, H. Ullmann, U. Guth, Solid State Ionics 175 (2004) 151.
[26] F.A. Kröger, The Chemistry of Imperfect Crystals, North-Holland, Amsterdam, 1974.
[27] R. Moos, K.H. Härdtl, J. Am. Ceram. Soc. 80 (1997) 2549.
[28] T. Bak, J. Nowotny, M. Rekas, C.C. Sorrell, J. Phys. Chem. Solids 64 (2003) 1057.
[29] S.M. Plint, P.A. Connor, S. Tao, J.T.S. Irvine, Solid State Ionics 177 (2006) 2005.